

## Numerical solution of Bloch's equation for neutron spin precession

P. A. Seeger<sup>a,\*</sup>, L. L. Daemen<sup>b</sup>

<sup>a</sup>239 Loma del Escolar, Los Alamos, NM 87544, USA

<sup>b</sup>Manuel Lujan Jr. Neutron Scattering Center, Los Alamos National Laboratory,  
Los Alamos, NM 87545, USA

### Abstract

The increasing importance of polarization in neutron scattering instrumentation for condensed matter research means that Monte Carlo design tools must be able to track neutron spin during neutron transport. In particular, we must be able to solve Bloch's precession equation for arbitrary magnetic induction configurations, including time-dependence. Since Monte Carlo simulations require averaging a large number of neutron histories, the computational procedure must be fast, as well as accurate and precise. A suitable algorithm is presented here, in the context of the Neutron Instrument Simulation Package (NISP), a Monte Carlo package developed at Los Alamos National Laboratory for neutron scattering instrument design. Accuracy is assessed by comparison to simple cases for which analytical expressions are known, and precision and execution time are shown for a case with a non-uniform magnetic induction field.

*PACS:* 03.75.Be, 13.88.+e, 29.27.Hj

*Keywords:* Neutron, polarization, Monte Carlo

\*Corresponding author.

*E-mail address:* PASeeger@aol.com

## 1. Introduction

The Neutron Instrument Simulation Package (NISP) is a set of programs including a web-based application for instrument description and a Monte Carlo engine to run simulations in the user's computer [1-4]. The programs and documentation are accessed at <http://strider.lansce.lanl.gov/NISP/Welcome.html>. In NISP, a "region" is defined in relation to general quadratic surfaces, and the algorithms for the material or device within the region are found in a subroutine library. A special feature is regions that describe magnetic induction. These may overlap and coexist with the material and device regions; any component may be placed in a magnetic field.

Neutron beam polarization is represented by a 3-vector  $\mathbf{P}$ , with magnitude  $P \leq 1$  [5,6]. The probability of the spin of the neutron being in direction  $\mathbf{P}$  is  $(1 + P)/2$ , and the probability of the opposite spin is  $(1 - P)/2$ . Thus  $P = 0$  is an unpolarized beam, with probability in *any* direction being 50%. Because of the quantum-mechanical nature of spin, any beamline component that is sensitive to neutron spin will have an orientation described by a unit vector  $\mathbf{n}$ . The probability that any particular neutron in the beam will interact with spin parallel to  $\mathbf{n}$  is  $(1 + \mathbf{n} \cdot \mathbf{P})/2$  and the anti-parallel probability is  $(1 - \mathbf{n} \cdot \mathbf{P})/2$ . In a Monte Carlo simulation, the component may *either* split the neutron into two independent histories with statistical weights multiplied by the respective probabilities, *or* it may use a random number to select one spin or the other based on the relative probabilities. The interaction may result in a different direction or magnitude of  $\mathbf{P}$ . Any operation that is symmetric with respect to spin, such as precession or spin-flip, can be applied either to the combined or to the separated histories. For algorithms that act differently on the two spin states, the single history must be decomposed; after the

interaction, the two histories may either remain separated or (only if the directions of  $\mathbf{P}$  are the same) may be recombined.

When computing transport of polarized neutrons, we must be able to calculate spin precession. Bloch's equation for the precession of neutron spin in a magnetic induction field is [7]

$$\frac{d\mathbf{P}}{dt} = -g_n \mathbf{P} \times \mathbf{B} \quad , \quad (1)$$

where  $\mathbf{P}$  is the polarization vector,  $d\mathbf{P}$  is the precession angle (orthogonal to  $\mathbf{P}$ ),  $\mathbf{B}$  is the magnetic induction vector (in units of T), and  $g_n$  is the neutron gyromagnetic ratio ( $-183.247 \text{ rad } \mu\text{s}^{-1} \text{ T}^{-1}$ ). Since  $g_n$  is negative, the precession will be right-handed about the  $\mathbf{B}$  axis. The precession of each neutron will be computed deterministically, and Monte Carlo will be used to average over all possible neutron trajectories.

As a neutron traverses a region with non-zero magnetic induction, it experiences a field varying in direction and intensity. From the viewpoint of the neutron, these variations are experienced as a time-dependent field. The particular time variation depends on the trajectory the neutron follows through the field. (We neglect any effect of the field on the neutron equation of motion.) In addition to this *implicit* time-dependence related to motion, the magnetic induction can also have an *explicit* time-dependence; this will be especially true at pulsed sources where optical devices may be designed with  $B$  proportional to the nominal neutron velocity. The notation  $\mathbf{B} = \mathbf{B}(t)$  encompasses both the explicit and implicit time dependence of the magnetic induction. Notice that the problem at hand is quite different from the situation encountered in Nuclear Magnetic Resonance where the magnetic induction is typically a superposition of harmonic and constant fields

with direction fixed in space. (The Bloch equations also include a relaxation term that is not relevant to the present discussion.)

As in the work of Halpern and Holstein [8], we choose the independent variable to be the magnetic field integral  $S$  (in radians), such that

$$S(t) = -g_n \int_0^t B(t) dt \quad , \quad (2)$$

$$dS = -g_n B(t) dt \quad . \quad (3)$$

The Larmor precession frequency is  $dS/dt$ . Any integrable function is allowed for  $B(t)$ , including zeros and sign changes. (Discontinuities are allowed, but are not treated as such because of the implicit assumption that length scales are large compared to the neutron wavelength.) The entire dependence of the precession on the strength of  $\mathbf{B}$  is a function of the line integral of  $B(t)$  along the neutron trajectory. It is also necessarily true that the magnitude of  $\mathbf{P}$  will not vary along the path, since  $dP^2/dt = 2 \mathbf{P} \cdot d\mathbf{P}/dt \equiv 0$ .

## 2. Direction of $\mathbf{B}$ constant

We first treat the case when the direction of the  $\mathbf{B}$  vector at all points along the neutron trajectory is constant:

$$\mathbf{B}(t) = B(t) \hat{\mathbf{b}} \quad , \quad (4)$$

where the time dependence includes space variations along the neutron path, and the unit vector  $\hat{\mathbf{b}}$  does not change. This case has an analytic solution, but leads to the derivation of the numerical algorithm in the next section. Bloch's equation becomes

$$\frac{d\mathbf{P}}{dS} = \begin{pmatrix} 0 & b_z & -b_y \\ -b_z & 0 & b_x \\ b_y & -b_x & 0 \end{pmatrix} \begin{pmatrix} P_x \\ P_y \\ P_z \end{pmatrix} . \quad (5)$$

This system of three 1<sup>st</sup> order coupled differential equations (with  $\hat{\mathbf{b}}$  is constant) can be shown to be equivalent to

$$\frac{d^3 \mathbf{P}}{dS^3} + \frac{d\mathbf{P}}{dS} = 0 \quad . \quad (6)$$

The solution of this equation is of the form

$$\mathbf{P}(S) = \mathbf{a} + \mathbf{C} \cos S - \mathbf{D} \sin S \quad , \quad (7)$$

with the nine coefficients of  $\mathbf{a}$ ,  $\mathbf{C}$ , and  $\mathbf{D}$  to be fitted to the initial conditions. We have chosen the (arbitrary) sign of  $\mathbf{D}$  to be negative because NISP uses a left-handed coordinate system, and it will subsequently be convenient to use  $-S$  for the precession angle.

Consider  $P_x(S=0)$ :

$$\begin{aligned} P_x(0) &= a_x + C_x = P_{0x} \quad , \\ P'_x(0) &= -D_x = b_z P_{0y} - b_y P_{0z} \quad , \\ P''_x(0) &= -C_x \quad . \end{aligned} \quad (8)$$

Thus by knowing  $\mathbf{P}_0$  and the direction  $\hat{\mathbf{b}}$  we already know the initial value of the component and its 1<sup>st</sup> derivative. Manipulation of the 2<sup>nd</sup> derivative to satisfy Bloch's equation gives  $a_x = b_x \hat{\mathbf{b}} \cdot \mathbf{P}_0$ . Combining the three components,

$$\begin{aligned} \mathbf{a} &= (\hat{\mathbf{b}} \cdot \mathbf{P}_0) \hat{\mathbf{b}} \quad , \\ \mathbf{C} &= \mathbf{P}_0 - \mathbf{a} \quad , \\ \mathbf{D} &= -\mathbf{P}_0 \times \hat{\mathbf{b}} \quad . \end{aligned} \quad (9)$$

Equations (2), (7), and (9) are the complete solution of Bloch's equation for arbitrary spatial and time variation of  $\mathbf{B}$ , in the special case that the direction of  $\mathbf{B}$  is constant at all points along the neutron trajectory.

### 3. Direction of $\mathbf{B}$ varies with $S$

When the direction of  $\mathbf{B}$  does vary, numerical integration may be used with stepsize depending on the rate of rotation of  $\mathbf{B}$ . This is non-trivial because the equations are “stiff,” meaning that there are two widely different time constants: in general, the rate of precession ( $S$ ) is much faster than the secular variations of  $\mathbf{B}(S)$ .

We can decompose the vector  $\mathbf{P}(S)$  into vectors  $\boldsymbol{\alpha}(S)$  and  $\boldsymbol{\beta}(S)$  that are respectively parallel and orthogonal to  $\mathbf{B}$ . Only  $\boldsymbol{\beta}$  undergoes precession. Thus

$$\begin{aligned}\mathbf{P}(S) &= \hat{\mathbf{a}}(S) + \hat{\mathbf{a}}(S) \\ &= P \cos \varrho \hat{\mathbf{b}} + P \sin \varrho \hat{\mathbf{a}} \quad ,\end{aligned}\tag{10}$$

where  $P$  is the constant magnitude of  $\mathbf{P}$  and  $\varrho$  is the slowly varying angle between  $\mathbf{P}$  and  $\mathbf{B}$ . Vector  $\boldsymbol{\beta}$  will include the rapid precession (proportional to  $S$ ) and also a slowly varying phase angle,  $\varphi$ . To define the phase angle unambiguously, we will rotate  $\mathbf{B}$  to lie on the  $Z$ -axis, so that the orthogonal vector  $\boldsymbol{\beta}$  will lie in the  $X$ - $Y$  plane. The rotation matrix  $R$  is found by first rotating the coordinate axes about  $Z$  by an angle  $C = -\tan^{-1}(b_x/b_y)$  to make  $b_x = 0$ , then rotating the vector about  $X$  by  $\gamma = -\cos^{-1}(b_z)$  to make  $b_z = 1$ , and finally rotating the axes about  $Z$  by  $-C$  to return to the original coordinate system. The result is

$$R = \begin{pmatrix} \cos C & -\sin C & 0 \\ \sin C & \cos C & 0 \\ 0 & 0 & 1 \end{pmatrix} \begin{pmatrix} 1 & 0 & 0 \\ 0 & \cos \gamma & \sin \gamma \\ 0 & -\sin \gamma & \cos \gamma \end{pmatrix} \begin{pmatrix} \cos C & \sin C & 0 \\ -\sin C & \cos C & 0 \\ 0 & 0 & 1 \end{pmatrix}.$$

After multiplying, expressing the trigonometric functions as ratios of components of  $\hat{\mathbf{b}}$ , and using the identity  $b_x^2 + b_y^2 + b_z^2 = 1$ , this becomes

$$R = \begin{pmatrix} R_{11} & R_{12} & -b_x \\ R_{12} & R_{22} & -b_y \\ b_x & b_y & b_z \end{pmatrix}, \tag{11}$$

where

$$\begin{aligned} R_{11} &= 1 - b_x^2 / (1 + b_z) \quad , \\ R_{12} &= -b_x b_y / (1 + b_z) \quad , \\ R_{22} &= 1 - b_y^2 / (1 + b_z) \quad . \end{aligned} \tag{12}$$

The limits of  $R_{11}$ ,  $R_{12}$ , and  $R_{22}$  as  $b_z$  approaches  $\pm 1$  are respectively 1, 0, and 1; no rotation is required in those cases, except for a sign flip when  $b_z = -1$ . Reversing the order of rotations gives the inverse of the matrix:

$$R^{-1} = \begin{pmatrix} R_{11} & R_{12} & b_x \\ R_{12} & R_{22} & b_y \\ -b_x & -b_y & b_z \end{pmatrix} . \tag{13}$$

Multiplying  $R$  times the initial value of  $\boldsymbol{\beta}$  defines  $f_0$ :

$$R \hat{\mathbf{a}}_0 = \frac{1}{P \sin \varrho} \begin{pmatrix} R_{11} b_{x0} + R_{12} b_{y0} - b_x b_{z0} \\ R_{12} b_{x0} + R_{22} b_{y0} - b_y b_{z0} \\ \mathbf{b} \cdot \hat{\mathbf{a}}_0 \end{pmatrix} \equiv \begin{pmatrix} \cos f_0 \\ \sin f_0 \\ 0 \end{pmatrix} . \tag{14}$$

(This definition fails when  $\sin \varrho = 0$ ; in that case, however,  $\boldsymbol{\beta} = 0$  so there is no precession and  $\mathbf{P} = \boldsymbol{\alpha}$  remains constant.) Precession as a function of  $S$  is a rotation of  $\boldsymbol{\beta}$  by an amount  $S$  in this X-Y plane. Since the coordinate system in NISP is left-handed, the right-handed precession about Z is represented by a negative phase angle. Replace  $f$  by  $(f - S)$  and multiply by  $R^{-1}$  to return to unrotated coordinates:

$$\begin{aligned} \hat{\mathbf{a}}(S) &= R^{-1} \begin{pmatrix} \cos(f - S) \\ \sin(f - S) \\ 0 \end{pmatrix} \\ &= \begin{pmatrix} R_{11} \cos f + R_{12} \sin f \\ R_{12} \cos f + R_{22} \sin f \\ -b_x \cos f - b_y \sin f \end{pmatrix} \cos S - \begin{pmatrix} R_{12} \cos f - R_{11} \sin f \\ R_{22} \cos f - R_{12} \sin f \\ -b_y \cos f + b_x \sin f \end{pmatrix} \sin S . \end{aligned} \tag{15}$$

The relationship to the vectors  $\mathbf{C}$  and  $\mathbf{D}$  in Eq. (7) for induction fields with constant direction is clear. Now, however, the nine coefficients of Eq. (9) have been reduced to three independent variables:  $P$ ,  $q$ , and  $f$ . Of these, amplitude  $P$  is constant and angles  $q$  and  $f$ , which depend *only* on the *direction* of the magnetic induction vector along the neutron trajectory, are assumed to vary slowly compared to the precession rate. (If the variation is too fast, then the integration of the differential equations remains stiff and execution time may not improve.)

We now need to develop the derivatives of  $q$  and  $f$ . Consider

$$\frac{d}{dS} \begin{pmatrix} x \\ y \\ z \end{pmatrix} = \frac{1}{P \sin q} R \frac{d\hat{\mathbf{a}}}{dS} = \frac{1}{P \sin q} R \frac{d}{dS} (\mathbf{P} - \hat{\mathbf{a}}) . \quad (16)$$

But  $d\alpha/dS = 0$ , and  $d\mathbf{P}/dS$  may be evaluated by Bloch's equation. Keeping  $\hat{\mathbf{b}}$  to represent the *initial* induction direction used to define the coordinate rotation, and letting  $\mathbf{B}(S)$  represent the induction at another point on the trajectory, we have

$$\frac{d}{dS} \begin{pmatrix} x \\ y \\ z \end{pmatrix} = \frac{1}{B P \sin q} R (\mathbf{P} \times \mathbf{B}) . \quad (17)$$

The component  $dz/dS$  is parallel to  $\hat{\mathbf{b}}$  and hence gives the change of  $\mathbf{P} \cdot \hat{\mathbf{b}}$ :

$$\begin{aligned} \frac{d}{dS} (P \cos q) &= P \sin q \frac{dz}{dS} \\ &= \frac{1}{B} \left[ b_x (P_y B_z - P_z B_y) + b_y (P_z B_x - P_x B_z) + b_z (P_x B_y - P_y B_x) \right] . \end{aligned} \quad (18)$$

This derivative is initially zero, and is also zero whenever  $\mathbf{B}$  is parallel to the initial  $\hat{\mathbf{b}}$ . Note that whenever the value of  $P \cos q$  is changed, then the value of  $P \sin q$  must also be adjusted. The angle  $f(S)$  is given by [cf. Eq. (15)]:

$$f(S) = S + \tan^{-1}(y/x) \quad , \quad (19)$$

$$\frac{df}{dS} = 1 + \sin(f - S) \frac{dy}{dS} - \cos(f - S) \frac{dx}{dS} \quad . \quad (20)$$

This derivative is also identically zero as long as  $\mathbf{B}$  is parallel to the initial  $\hat{\mathbf{b}}$ , since then  $dy/dS = -\sin(f - S)$  and  $dx/dS = \cos(f - S)$ . Expanding Eq. (17) to show the terms for Eq. (20) explicitly,

$$\begin{aligned} \frac{dx}{dS} &= \frac{1}{BP \sin \varrho} \left[ R_{11} (P_y B_z - P_z B_y) + R_{12} (P_z B_z - P_x B_z) - b_x (P_x B_y - P_y B_x) \right] \quad , \\ \frac{dy}{dS} &= \frac{1}{BP \sin \varrho} \left[ R_{12} (P_y B_z - P_z B_y) + R_{22} (P_z B_z - P_x B_z) - b_y (P_x B_y - P_y B_x) \right] \quad . \end{aligned} \quad (21)$$

In these expressions the values of  $R_{11}$ ,  $R_{12}$ , and  $R_{22}$  are from Eq. (12).

#### 4. Integration

For either the parallel field of Sec. 2 or the variable-direction case of Sec. 3, it is essential to obtain an accurate evaluation of  $S$  from Eq. (2). Applying a Runge-Kutta integration with error control and adaptive stepsize [9] directly using the derivatives of Eqs. (18) and (20), the stepsize would always be reduced to track variations in  $S$ . This causes many more evaluations of the derivatives than are really necessary. Since in a Monte Carlo simulation many millions of neutrons may be tracked, it is important to make the code as fast as possible; thus the stepsize for the line integral of Eq. (2) must be decoupled from the integration of Bloch's equation.

Since it also may be time consuming to compute the magnetic induction at arbitrary points on the trajectory, the integration method chosen for Eq. (2) must be efficient. We use Romberg's algorithm [10]. This uses extended trapezoidal integration with stepsize  $h$  reduced by a factor of 2 at each stage, with the resulting table  $s(h^2)$  being extrapolated to

$h^2 = 0$  to give the estimated integral. Step size division continues until the new term added to  $s(h^2)$  is less than a specified absolute error. The first approximation is Simpson's Rule, but higher orders are pursued until the error requirement is met. The Fortran-coded function BINTEGRAL may be obtained from the NISP web site [11]. The magnetic induction at time  $t$  along the trajectory is computed by a user-supplied function that returns  $B(t)$  as its value; the vector  $\mathbf{B}(t)$  is also returned in the calling sequence of the function. Input to the function includes the particle trajectory and a parameter array. Examples may be found attached to subroutine BFIELD.

The differential equations are integrated using a fourth-order Runge-Kutta procedure [10]. The step size manager (RKPRECES) is straightforward, comparing the computed  $\mathbf{P}$  for the full step to the value obtained in two half steps, and demanding that the difference in every component of  $\mathbf{P}$  be less than a specified value  $\epsilon$  (we are presently using  $\epsilon = 3 \times 10^{-4}$ ; see Sec. 6 below). The Runge-Kutta stepper routine, RK4BLOCH, is highly specialized and may be downloaded from the NISP web site [11]. Equations (10), (12), and (18)-(21) are coded explicitly; the only external function required is the one to compute  $\mathbf{B}(t)$  along the trajectory. When BINTEGRAL is called from RK4BLOCH, the error parameter passed is  $\epsilon/|g|$ . [Note that in the program listing, variable "phi" represents  $(f - S)$ , so its derivative is  $df/dS - 1$ . Also, vector "beta" in the code is the unit vector  $\boldsymbol{\beta} / P \sin\alpha$ .]

## 5. Examples

We give examples for two cases with analytic solutions, as a test of accuracy, and then study a case with a strongly varying field to estimate precision.

### A. Adiabaticity coefficient

The adiabaticity coefficient  $E$  is the ratio of the Larmor precession frequency to the rate of rotation of the magnetic field. A large value of the coefficient means that the neutron precession is fast enough that the polarization direction will track the field change; a small value does not give the neutron enough time to reorient. Consider a field  $\mathbf{B}$  that rotates uniformly from the +Y direction to the +X direction (with constant magnitude) and a neutron initially polarized parallel to  $\mathbf{B}$ . If the time for the neutron to traverse the region is  $\Delta t$ , then

$$E = \frac{dS / dt}{(\mathbf{p} / 2) / \Delta t} = \frac{2}{\mathbf{p}} (-g_n B) \Delta t . \quad (22)$$

Thus adiabaticity is inversely proportional to neutron velocity. When the neutron emerges from the field, component  $P_x$  will be 1 if the spin tracks the field rotation. The analytic expression for  $P_x$  is [12]

$$P_x(E, \mathbf{p} / 2) = \left[ E^2 + \cos\left(\frac{\mathbf{p}}{2} \sqrt{1 + E^2}\right) \right] / (1 + E^2) . \quad (23)$$

In Fig. 1 we compare this expression and the corresponding expressions for  $P_y$  and  $P_z$  to the numerical integration of the components of  $\mathbf{P}$  for a range of neutron velocities. The *rms* deviations of the numerical from analytical results respectively for  $P_x$ ,  $P_y$ , and  $P_z$  are  $5 \times 10^{-5}$ ,  $7 \times 10^{-4}$ , and  $6 \times 10^{-4}$ . This shows that the numerical procedure is able to track field variations at small adiabaticity very accurately.

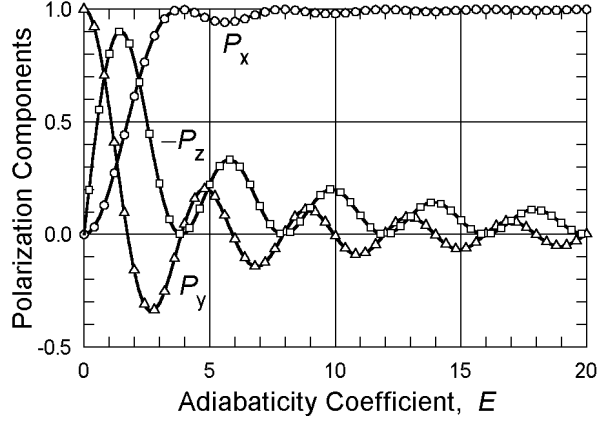


Fig. 1. Components of  $\mathbf{P}$  for a neutron initially polarized parallel to  $\mathbf{B}$ , after a rotation of  $\mathbf{B}$  by  $\pi/2$  from +Y to +X. Symbols are integrated numerically, and the lines are analytic. The adiabaticity coefficient is the ratio of the neutron precession frequency to the rate of rotation of  $\mathbf{B}$ . Component  $P_z$  is negative because of our use of a left-handed coordinate system.

### B. Majorana flipping

The situation of a polarized (atomic) beam passing near a null point in a field with a strong gradient was considered by Majorana [13]. He defines a scale parameter in terms of the gradient of the parallel field and the magnitude of the residual transverse component at the field minimum:

$$k = -g_n \frac{B_{\perp}^2}{dB/dt} = -g_n \frac{B_{\perp}^2}{\Delta B} \Delta t \quad . \quad (24)$$

This is similar to the adiabaticity coefficient of Eq. (22); it is inversely proportional to neutron velocity or proportional to wavelength. The matrix element for the spin *not* to track the change of sign of the field (which Majorana considers to be reorientation) is  $W(-) = \exp(-k \rho/2)$ ; in terms of our notation for average spin this becomes

$$P_{final} / P_{initial} = W(-) - W(+) = 2 \exp(-k \rho/2) - 1 \quad , \quad (25)$$

where  $P$  refers to the component of  $\mathbf{P}$  parallel to the initial  $\mathbf{B}$ . Figure 2 shows the results of our test cases, with  $\mathbf{B}$  vertical and varying from +1 T to -1 T over a distance of 1 m. This strong field leads to a very high precession rate; the number of rotations at  $l = 30 \text{ \AA}$

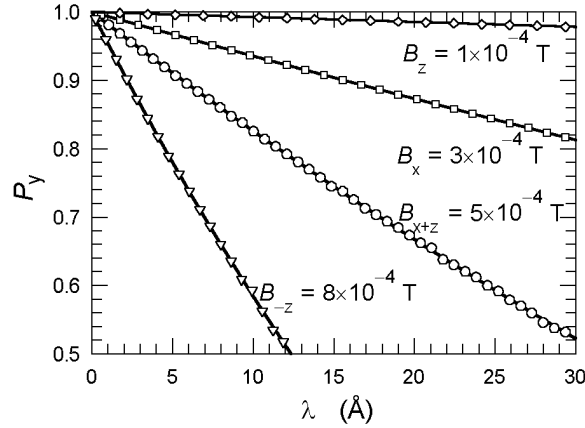


Fig. 2. Comparison of Majorana flipping curves (solid lines) to numerical integration of Bloch's equation (symbols). The gradient of the principal field  $B_y$  is 2 T/m, and values of the residual transverse fields are shown for each curve.

exceeds  $10^5$ . The average step of the Runge-Kutta integration covered 20 precessions. Many neutron velocities were computed for each of four values of  $B_{\perp}$  (all at different orientations): 1, 3, 5, and  $8 \times 10^{-4}$  T. Since our internal precision testing is per step, cases requiring more than 1000 integration steps have noticeable deviations from the theoretical curves. For the respective values of  $B_{\perp}$ , the *rms* deviations are 0.0002, 0.0007, 0.0014, and 0.0016. We deem this to be adequate accuracy for such a severe test.

### C. Current loop

One algorithm that has been implemented in NISP computes  $\mathbf{B}$  for any number of current loops [14]. For a test case, we used one loop of radius 50 mm, perpendicular to the Z-axis, centered on the axis, with various values of the current. We start a neutron 0.5 m in front of the loop and track it for 1 m. The neutron starts off-center ( $X = +10$  mm,  $Y = -2$  mm) and is moving at an angle ( $dX/dZ = +2.5$  mrad,  $dY/dZ = +1$  mrad), with a velocity of 400 m/s. Figure 3 is a plot of the computed  $\mathbf{B}$ . It can be seen that there is a considerable

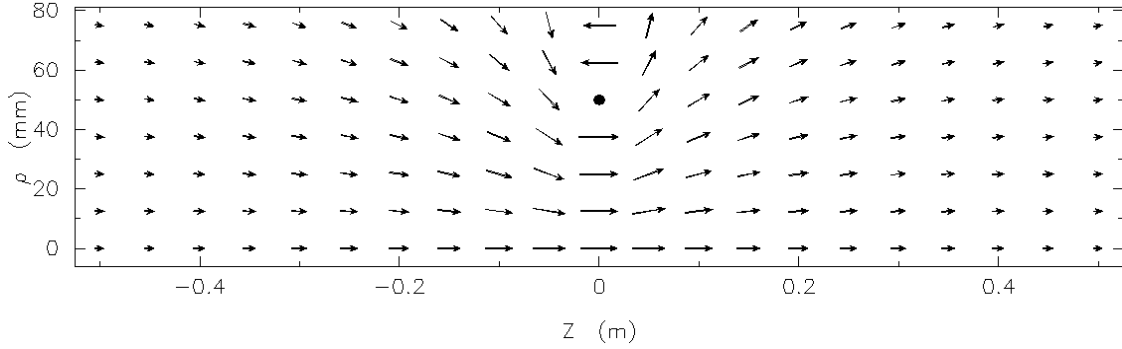


Fig. 3. Magnetic induction from a current loop. Although the vertical scale of the plot is exaggerated, the true directions of the  $\mathbf{B}$  vectors are shown. The magnitudes are logarithmic, with the vector length at  $(0, 0)$  representing 4 decades. That is, a vector of 0 length represents a value of  $B$  that is  $10^{-4}$  times as large;  $\frac{1}{4}$  the length is  $10^{-3}$ ,  $\frac{1}{2}$  the length is  $10^2$ , *etc.* The large dot is the location of the current-carrying wire.

fluctuation of the transverse field component as the neutron passes through the ring at 11.35 mm off-center. The value of  $B$  at the center of the loop is proportional to current:

$$B_0 = \frac{\mu_0 I}{2R} = (1.2557 \times 10^{-5} \text{ T/A}) I . \quad (26)$$

Values of  $I$  from 0.1 A to 10,000 A have been tested.

The initial polarization used for the neutron was  $(0.5, 0.5, 0.5^{1/2})$ , making the magnitudes of the precessing and non-precessing components nominally equal. Insofar as the direction of  $\mathbf{B}$  is not parallel to  $Z$ , the components mix and in particular the “desirable” component  $P_z$  may either increase or decrease, depending quite sensitively on the precise phase of the precession. The most extreme phase dependence occurred near a current of 10.87 A, for which the integral of  $B$  over the 1-m path produces exactly one precession revolution. This case is shown in Fig. 4, where the final  $P_z$  is plotted for various phase angles of the initial  $P_{0x}, P_{0y}$ . The average of the 24 computed initial phases gives precisely the same value of  $\mathbf{P}$  (all components) as a computation with the initial  $P_{0x} = P_{0y} = 0$ . This gives credence to the statement in Sec. 1 that the precession can be applied either to separated or combined histories.

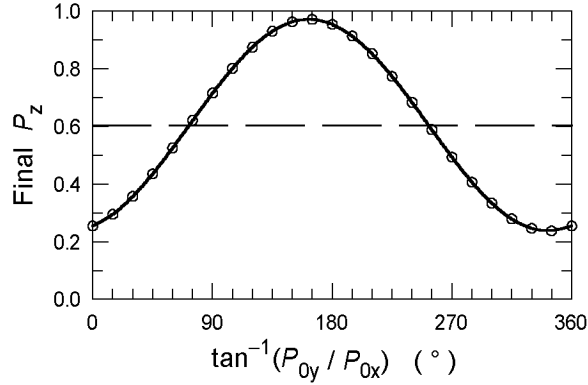


Fig. 4. Dependence of final  $P_z$  on the phase of the transverse component of  $\mathbf{P}_0$ . The loop current is 10.87 A, so that the neutron undergoes one precession revolution. The dashed line is for “random” phase,  $P_{0x} = P_{0y} = 0$ , and has the same value, 0.6044, as the average of the computed phases with  $P_{0x}^2 + P_{0y}^2 = 0.5$ .

Results of tracking  $P_z$  while the neutron passes through the current loop are shown for three loop currents in Fig. 5. As the current increases, there are large oscillations in  $P_z$  at the precession frequency. To see how the  $q-f$  coordinates vary in this example, we have added up the changes in the angles across each Runge-Kutta step and the plotted cumulative  $\Delta q$  and  $\Delta f$  in Fig. 6. Then to verify the statement that  $q$  and  $f$  vary slowly with  $S$ , the same  $\Delta q$  and  $\Delta f$  values have been plotted against the cumulative  $S$  in Fig. 7. In these two figures the dots on the  $\Delta f$  line are the adaptive Runge-Kutta steps generated

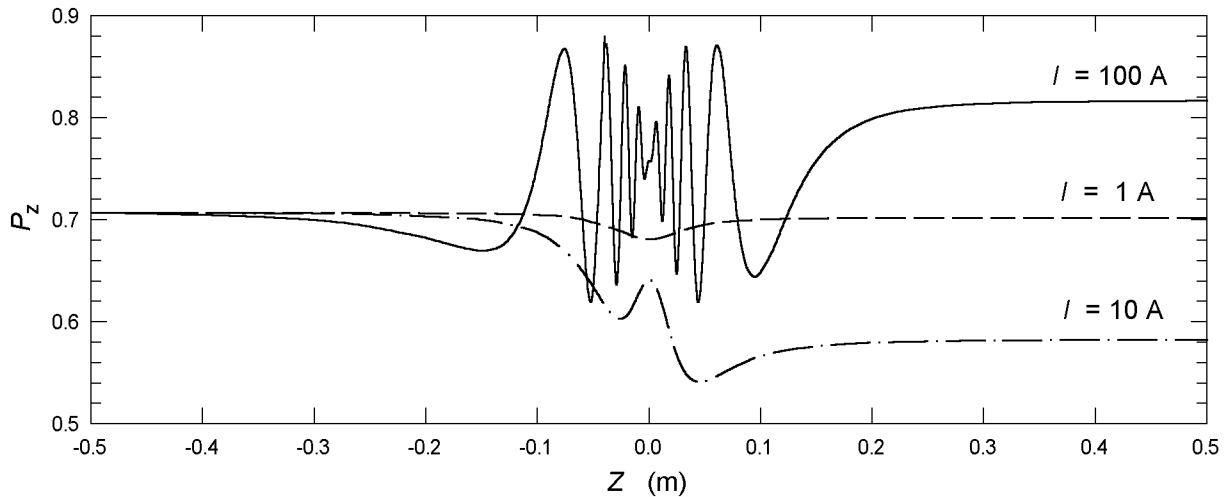


Fig. 5. Z-component of polarization of neutrons with initial  $\mathbf{P}_0 = (-0.5, -0.5, +0.7071)$ , passing off-center through current loops with various currents,  $I$ .

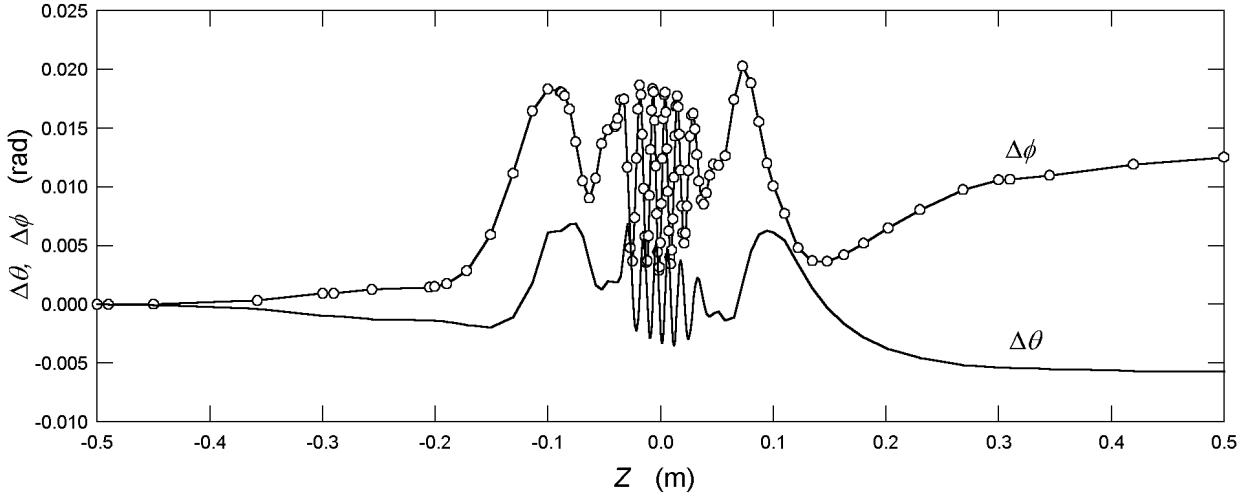


Fig. 6. Cumulative variation of  $q$  and  $f$  angles for the case  $I = 100$  A (cf. Fig. 5). The points on the  $\Delta\phi$  line indicate the steps in the Runge-Kutta integration of Eqs. (18) and (20).

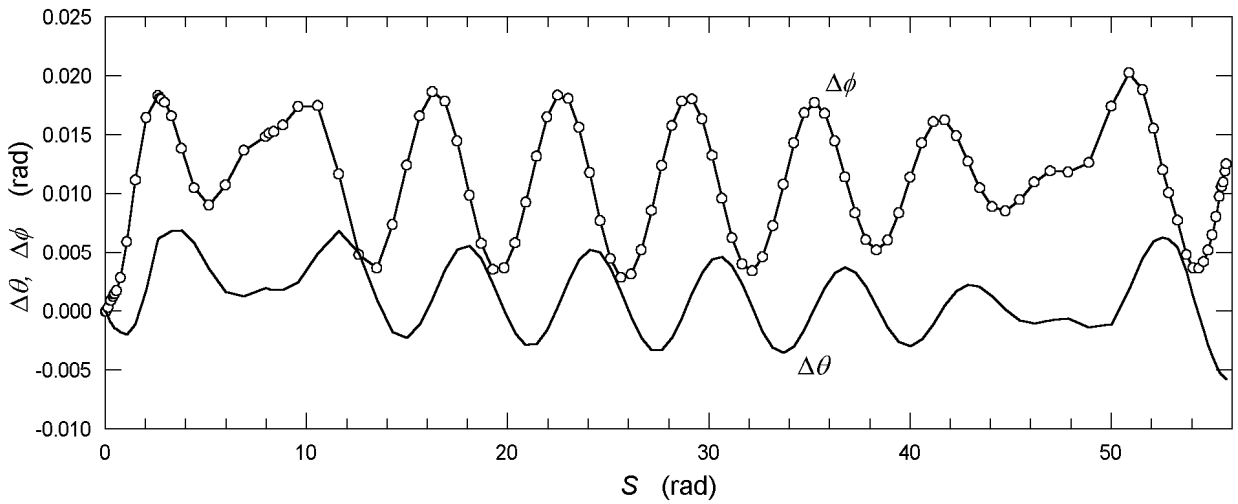


Fig. 7. Data of Fig. 6, plotted vs.  $S$  from eq. (2), showing that amplitudes of the variations  $\Delta q$  and  $\Delta f$  are small compared to  $S$ .

by the program. Both  $\Delta q$  and  $\Delta f$  are quasi-periodic on  $2\rho S$ , but the amplitudes are indeed small.

### 6. Precision and execution time

To optimize the code for use in Monte Carlo simulations, the tradeoff between precision and execution time must be explored. We have compared results for values of the absolute error parameter  $\epsilon$  from  $1 \times 10^{-5}$  to  $3 \times 10^{-2}$ . For each  $\epsilon$ , the current-loop

example of Sec. 5C was run at six currents from 0.1 A to 10,000 A. The sum of the absolute deviations of the final  $P_z$  for the six currents, compared to the values at the smallest  $\epsilon$ , was taken as a measure of precision. The results are shown in Fig. 8, along with the sum of the six execution times (on a 600-MHz Pentium III processor). Based on this plot, we have chosen  $\epsilon = 3 \times 10^{-4}$ . In the current version of NISP, this is set in a parameter statement in subroutine BFIELD. Further experience may lead us to change the value of  $\epsilon$ , or to make it more easily available to be modified at run time. The execution times and the results of the six individual cases are given in Table 1. The maximum depolarization (minimum final  $P_z$ ) occurs when the number of precessions ( $S/2p$ )  $\approx 1$ .

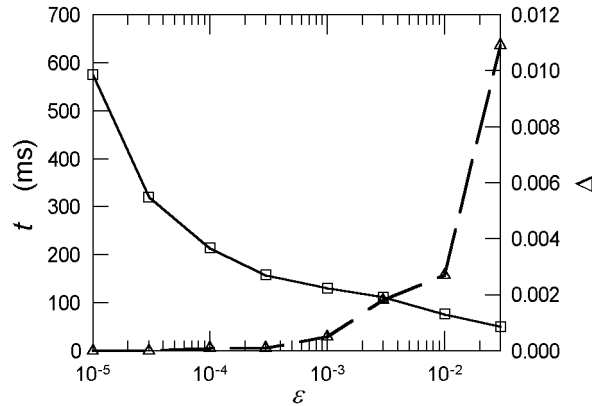


Fig. 8. Precision and execution time as functions of the absolute error parameter  $\epsilon$ . Execution time (squares, left scale) is the sum of six current-loop cases, on a 600-MHz Pentium III processor. The precision (triangles, right scale) is defined as the sum of the absolute deviations of  $P_z$  from the values with  $\epsilon = 1 \times 10^{-5}$ .

## 7. Conclusions

The aim of this study was to find a procedure for solving Bloch's precession equation that is accurate and precise, and also fast enough to be used with a Monte Carlo simulation package (specifically, NISP, <http://strider.lansce.lanl.gov/NISP/Welcome.html>). The method described and the subroutines provided at the web site [11] meet this need.

Table 1. Results and execution times for neutrons passing off-center through loops with various currents. Initial polarization (0, 0, 0.7071).

| $I$<br>(A) | $P_x$   | $P_y$   | $P_z$  | $S / 2p$ | Execution<br>(ms) |
|------------|---------|---------|--------|----------|-------------------|
| 0.1        | -0.0002 | -0.0001 | 0.7071 | 0.009    | 1.19              |
| 1.0        | -0.0073 | 0.0050  | 0.7071 | 0.092    | 2.05              |
| 10.0       | 0.3657  | -0.0220 | 0.6048 | 0.920    | 3.9               |
| 100        | 0.0697  | -0.0925 | 0.6976 | 9.197    | 10.8              |
| 1000       | 0.0506  | -0.0120 | 0.7052 | 91.972   | 30.2              |
| 10,000     | 0.0313  | 0.0166  | 0.7062 | 919.719  | 110               |

### Acknowledgements

We would like to thank Trefor Roberts of the Institut Laue-Langevin for many useful suggestions, especially the analytic comparisons. This work was supported in part by the Manuel Lujan Jr. Neutron Scattering Center, a national user facility funded by the United States Department of Energy, Office of Basic Energy Sciences–Materials Science, under contract number W-7405-ENG-36 with the University of California.

### References

- [1] P. A. Seeger, in Proceedings of the 13<sup>th</sup> Meeting of the International Collaboration on Advanced Neutron Sources, PSI Proceedings 95-02, ISSN 1019-6447 (1995), pp. 194-212; T. G. Thelliez, L. L. Daemen, P. A. Seeger, and R. P. Hjelm, Jr., *ibid.*, pp. 307-331.

- [2] P. A. Seeger, L. L. Daemen, T. G. Thelliez, and R. P. Hjelm, Jr., in Proceedings of the 14<sup>th</sup> Meeting of the International Collaboration on Advanced Neutron Sources, Argonne National Laboratory report ANL 98/33, ISSN 1560-859X (1998), pp. 202-218.
- [3] L. L. Daemen, P. A. Seeger, T. G. Thelliez, and R. P. Hjelm, Jr., AIP Conf. Proc. 479 (1999) 40; Proc. SPIE 3771 (1999) 80.
- [4] P. A. Seeger, L. L. Daemen, T. G. Thelliez, and R. P. Hjelm, Jr., Physica B 283 (2000) 433.
- [5] W.G. Williams, Polarized Neutrons, Clarendon Press, Oxford, 1988.
- [6] S. W. Lovesey, Theory of Thermal Neutron Scattering from Condensed Matter, Vol. 2, Clarendon Press, Oxford, 1984, Ch. 10.
- [7] F. Bloch, Phys. Rev. 70 (1946) 460.
- [8] O. Halpern and T. Holstein, Phys. Rev. 59 (1941) 960.
- [9] W. H. Press, B. P. Flannery, S. A. Teukolsky, and W. T. Vetterling, Numerical Recipes, Cambridge University Press, 1986, Sec. 15.1, 15.2.
- [10] W. H. Press, S. A. Teukolsky, W. T. Vetterling, and B. P. Flannery, Numerical Recipes, Second Ed., Cambridge University Press, 1992, Sec. 4.3.
- [11] Source codes for the complete MCLIB library are available by anonymous ftp from <ftp://strider.lansce.lanl.gov/pub/NISP/Fortran/> (which may be accessed through the web site <http://strider.lansce.lanl.gov/NISP/Welcome.html>), or you may contact the author by e-mail at [PASeeger@aol.com](mailto:PASeeger@aol.com).
- [12] R. R. Newton and C. Kittel, Phys. Rev. 74 (1948) 1604.
- [13] E. Majorana, Nuovo Cimento 9 (1932) 43.
- [14] E. Durand, Magnetostatique, Masson, Paris, 1968, p.30.

## FIGURE CAPTIONS

Fig. 1. Components of  $\mathbf{P}$  for a neutron initially polarized parallel to  $\mathbf{B}$ , after a rotation of  $\mathbf{B}$  by  $\pi/2$  from +Y to +X. Symbols are integrated numerically, and the lines are analytic.

The adiabaticity coefficient is the ratio of the neutron precession frequency to the rate of rotation of  $\mathbf{B}$ . Component  $P_z$  is negative because of our use of a left-handed coordinate system.

Fig. 2. Comparison of Majorana flipping curves (solid lines) to numerical integration of Bloch's equation (symbols). The gradient of the principal field  $B_y$  is 2 T/m, and values of the residual transverse fields are shown for each curve.

Fig. 3. Magnetic induction from a current loop. Although the vertical scale of the plot is exaggerated, the true directions of the  $\mathbf{B}$  vectors are shown. The magnitudes are logarithmic, with the vector length at (0, 0) representing 4 decades. That is, a vector of 0 length represents a value of  $B$  that is  $10^{-4}$  times as large;  $1/4$  the length is  $10^{-3}$ ,  $1/2$  the length is  $10^{-2}$ , *etc.* The large dot is the location of the current-carrying wire.

Fig. 4. Dependence of final  $P_z$  on the phase of the transverse component of  $\mathbf{P}_0$ . The loop current is 10.87 A, so that the neutron undergoes one precession revolution. The dashed line is for "random" phase,  $P_{0x} = P_{0y} = 0$ , and has the same value, 0.6044, as the average of the computed phases with  $P_{0x}^2 + P_{0y}^2 = 0.5$ .

Fig. 5. Z-component of polarization of neutrons with initial  $\mathbf{P}_0 = (-0.5, -0.5, +0.7071)$ , passing off-center through current loops with various currents,  $I$ .

Fig. 6. Cumulative variation of  $q$  and  $f$  angles for the case  $I = 100$  A (*cf.* Fig. 5). The points on the  $\Delta f$  line indicate the steps in the Runge-Kutta integration of Eqs. (18) and (20).

Fig. 7. Data of Fig. 6, plotted *vs.*  $S$  from eq. (2), showing that amplitudes of the variations  $\Delta q$  and  $\Delta f$  are small compared to  $S$ .

Fig. 8. Precision and execution time as functions of the absolute error parameter  $e$ . Execution time (squares, left scale) is the sum of six current-loop cases, on a 600-MHz Pentium III processor. The precision (triangles, right scale) is defined as the sum of the absolute deviations of  $P_z$  from the values with  $e = 1 \times 10^{-5}$ .